14

Self-Consistent Mean-Field Theory for Room-Temperature Ionic Liquids

Yansen Lauw[1] and Frans Leermakers[2]
[1]*CSIRO Process Science and Engineering, Bayview Avenue, Clayton South, Victoria 3169*
Bragg Institute, ANSTO, PMB 1, Menai, NSW 2234
[2]*Laboratory of Physical Chemistry and Colloid Science, Wageningen University, Dreijenplein 6, Wageningen 6700 EK*
[1]*Australia*
[2]*The Netherlands*

1. Introduction

Research in room-temperature ionic liquids (RTILs) has exploded in the last two decades, which are marked by an exponential increase in the number of theoretical and experimental publications in this field. The typically good thermal stability, ionic conductivity, and solvability of RTILs make them superior electrolytes in many electrochemical applications, such as metal electrodeposition and energy storage.(Armand et al., 2009; Endres et al., 2008; Ohno, 2005; Simon & Gogotsi, 2008) The efficiency of RTILs in such applications is determined by a number of factors, one of which is the relationship between the interfacial structure of RTILs and their electrochemical properties. The use of RTILs as solvents in supercapacitors is of particular interest since they can generate significant electrical double-layer (EDL) capacitance due to the formation of thin layer of ions on an Angstrom-scale at RTIL-electrode interfaces.(Atkin & Warr, 2007; Baldelli, 2008; Horn et al., 1988; Mezger et al., 2008; 2009; Rivera-Rubero & Baldelli, 2004; Santos et al., 2006; Yuan et al., 2010) The formation of ultra thin EDL is mainly caused by the absence of any solvation shells around RTILs, which also enhances the accessibility of ions to penetrate nanoporous electrodes, thus increasing their useability in electrochemical applications.(Chmiola et al., 2008; Largeot et al., 2008)

The precise form of EDL structure in RTILs has been a point of argument recently. Experimental results from the sum frequency generation spectroscopy suggest a monolayer of ion formed at the interface.(Baldelli, 2008; Rivera-Rubero & Baldelli, 2004) However, a similar study using the surface force apparatus,(Horn et al., 1988) atomic force microscopy,(Atkin & Warr, 2007; Atkin et al., 2009) and x-ray reflectometry (Mezger et al., 2009) indicate that an alternating layer of ions is instead present. Analytical and numerical models also predict the formation of alternating layer of counterions and coions on polar surfaces due to strong steric and electrostatic correlations in RTILs.(Fedorov & Kornyshev, 2008; Feng et al., 2009; Kornyshev, 2007; Lauw et al., 2009; 2010; Oldham, 2008; Reed et al., 2008) Such an alternating layer typically occurs through the so-called charge overcompensation/overscreening mechanism when the electrostatic screening length is practically less than the size of the ion.(Outhwaite et al., 1980; Parsons, 1990; Stillinger & Kirkwood, 1960) In the highly charged system like RTILs, the charge overcompensation

understandably occurs since the ions are rather bulky. At the RTIL-electrode interface, the surface charge would be overscreened by counterions in the Helmholtz layer and the resulting net charge would be further overcompensated by coions in the subsequent layer, and so on.
The formation of the EDL in RTILs at charged interfaces can induce a large electrostatic potential field ($\sim 10^9$ V/m), which would greatly influence the rate of electrochemical reactions at the interface and the overall EDL capacitance values. In general, the EDL capacitance reflects the extent to which the electrostatic potential at the interface is screened by the ions that accumulate there. A better screening is reflected by a higher capacitance value. This parameter contains a valuable information on the thickness of the EDL and the composition and polarization of ions at the interface. A correct analysis of the shape of the EDL capacitance curve in RTILs requires an *a priori* knowledge on the EDL structure as a function of the electrostatic potential field. Analytical model to study the relationship between the EDL structure and capacitance in RTILs has been carried out (Kornyshev, 2007; Oldham, 2008) using Poisson-Fermi equation to model spherical ions with certain excluded volume.(Bazant et al., 2009; Bikerman, 1942; Freise, 1952; Kilic et al., 2007) A similar study has been done using numerical model, such as molecular dynamic simulations,(Fedorov & Kornyshev, 2008; Feng et al., 2009) Monte Carlo simulations,(Trulsson et al., 2010) and the self-consistent mean-field theory (SCMFT).(Lauw et al., 2009; 2010) Numerical modelling techniques are generally more realistic to model RTILs than existing analytical approaches due to their ability to accommodate internal degree of freedoms in RTILs and complicated (non-spherosymmetrical) structures of RTILs. These aspects are typically not accessible in analytical models.
This chapter describes the use of SCMFT to predict the structure of RTILs at electrified interfaces and the corresponding EDL capacitance. Special attention is paid to study the effect of ion-size and specific (non-electrostatic) adsorption of ions on the shape of the EDL capacitance curve. Results from this study is used to shed light on the unusual shape of the differential capacitance curve in RTILs observed in experiments. In general, the capacitance curve in RTILs has a shape of inverse parabola or a camel-like with two maxima around the point of zero charge (pzc),(Alam et al., 2007; 2008; Lockett et al., 2008) which are in contrast to the parabola-shaped capacitance curve typically found in aqueous electrolytes.
In SCMFT, the EDL capacitance is studied based on a detailed molecular model of RTILs and the use of local (effective) dielectric constant. Each ion is modelled as a freely-jointed chain of segments. The local polarization is implemented by assigning a higher relative permittivity to polar (more conductive) components in RTILs and a lower value to less polar (less conductive) components. The effective relative permittivity, which depends on the local distribution of the polar and apolar components, is thus higher at the surface than in the bulk since the polar components of the counterion are accumulated on the electrode's surface. This is the opposite trend to the one typically found in aqueous electrolytes,(James & Healy, 1972; Teschke & de Souza, 1999) in which the ion polarizability is known to decrease in high electrostatic fields. Details of the SCMFT used to model RTILs at electrified interface are given in the following section.

2. Self-consistent mean-field theory

The SCMFT is a molecular modelling technique used to study physical and thermodynamic properties of systems at equilibrium.(Fleer et al., 1993; Leermakers et al., 2005) It has been successfully implemented in the past to predict the equilibrium structure in polymeric systems.(Claessens et al., 2004; Lauw et al., 2008; Lauw, 2009; Leermakers et al., 2003; Matsen,

1995; Thompson et al., 2001) Here, it is used to study RTILs by considering a grand canonical ensemble of small systems, in which each system consists of cations and anions adjacent to an electrified solid surface. A periodic boundary condition is applied to all sides perpendicular to the surface and a Neumann boundary condition on the side opposite to the surface to reflect bulk properties. Each ion is modelled as a chain of charged and uncharged segments which formed a tetramer, as shown in Fig. 1. This implies that the charged group is situated at the center and the uncharged segments are located at the arms of the tetramer. For the cation, the positively charged segment P is surrounded by four arms, where each arm is composed of n_A neutral segments A. For the anion, the negatively charged segment N is also surrounded by four arms, comprising n_B neutral segments B per arm. Each segment is identified by its ranking number s, which marks the position of the segment in the tetramer. The density of each segment at any points $\mathbf{r}$ in the system is quantified by its local volume fraction $\varphi(\mathbf{r})$. This relatively simple molecular model is a representation of typical RTILs with a similar ion-size and a well-hidden charged group.

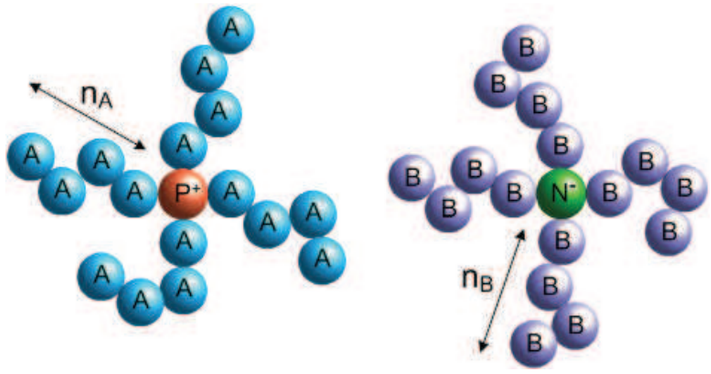

Fig. 1. Schematic of the tetrameric cation (left) and anion (right) used in the SCMFT.

In SCMFT, the total free energy (F_{total}) of a small system is expressed as a sum of its enthalpic, entropic, and electrostatic components,

$$F_{total} = F_{enthalphy} + F_{entropy} + F_{electrostatic} \tag{1}$$

The enthalpic part of the free energy reads,

$$\frac{F_{enthalphy}}{k_B T} = \int \left[\frac{1}{2} \sum_{i,j} \chi_{ij} \varphi_i(\mathbf{r}) \varphi_j(\mathbf{r}) + \delta(\mathbf{r} - \mathbf{r_S}) \sum_i \chi_{iS} \varphi_i(\mathbf{r}) \right] d\mathbf{r} \tag{2}$$

where the first term is the mixing enthalpy based on the Flory-Huggins formulation,(Flory, 1953) and the second term is originated from the specific adsorption. The indices i and j refer to the segment type in the cation and anion, i.e., $\{i, j\} \in \{A, P, B, N\}$; the index S represents the electrode's surface; χ_{ij} is the Flory-Huggins interaction parameter between segment-i and -j; $\varphi_i(\mathbf{r})$ and $\varphi_j(\mathbf{r})$ are the volume fraction of segment-i and -j at point $\mathbf{r}$ in the system; $\delta(\mathbf{r} - \mathbf{r_S})$ is the Dirac delta function at $\mathbf{r} = \mathbf{r_S}$, where $\mathbf{r_S}$ is the position of the electrode's surface; χ_{iS} is the interaction parameter between segment-i and the surface. A more positive χ_{iS} indicates a more repulsion between segment-i and the electrode's surface, and alternatively, a more negative χ_{iS} means segment-i has a stronger affinity towards the surface.

The entropic contribution to the total free energy is expressed as a sum of the translational entropy of the cation and anion, local mean-field interactions, and the additional term due to the incompressibility constraint of the system,

$$\begin{aligned}\frac{F_{entropy}}{k_BT} &= \frac{Vf_+}{N_+}\ln\left(\frac{Vf_+}{N_+Q_+}\right)+\frac{Vf_-}{N_-}\ln\left(\frac{Vf_-}{N_-Q_-}\right)\\ &\quad -\int\left[\sum_i w_i(\mathbf{r})\varphi_i(\mathbf{r})+\lambda(\mathbf{r})\left(1-\sum_i\varphi_i(\mathbf{r})\right)\right]d\mathbf{r}\end{aligned} \tag{3}$$

In Equation 3, the volume of the system is denoted by V; the indices $+$ and $-$ represent the cation and anion, respectively; f_+ and f_- are the total (volume) fraction of the cation and anion; N_+ and N_- are the total number of segments in the cation and anion; Q_+ and Q_- are the so-called partition function of the cation and anion; $w_i(\mathbf{r})$ is the potential of mean-force of segment-i at $\mathbf{r}$ and $\lambda(\mathbf{r})$ is the Lagrange multiplier at $\mathbf{r}$.
The electrostatic contribution to the free energy is expressed as a sum of all Coulombic interactions in the system as follows,

$$\frac{F_{electrostatic}}{k_BT}=-\frac{1}{2}\int\sum_i e\nu_i\varphi_i(\mathbf{r})\psi(\mathbf{r})d\mathbf{r} \tag{4}$$

where ν_i is the valence of segment-i and $\psi(\mathbf{r})$ is the electrostatic potential at $\mathbf{r}$.
The total free energy F_{total} is extremized with respect to the order parameters ($w_i(\mathbf{r})$ and $\varphi_i(\mathbf{r})$), subject to the incompressibility constraint $\sum_i\varphi_i(\mathbf{r})=1$ at all $\mathbf{r}$. The results is a set of governing equations described in details below.
For the cation, the volume fraction of each segment is determined by the corresponding segment-weighting factor $q_+(\mathbf{r},s)$ and its complementary factor $q'_+(\mathbf{r},s)$. They quantify the probability to find a given segment in the cation with a ranking number s at point $\mathbf{r}$ in the system. The segment-weighting factor $q_+(\mathbf{r},s)$ is calculated from the open-end of the arm towards the center of the tetramer, whereas the complementary segment-weighting factor $q'_+(\mathbf{r},s)$ is calculated from the center of the tetramer towards the open-end of the arm. The overall connectivity of segments is governed by the Edwards diffusion equation,(Edwards, 1965)

$$\frac{\partial q(\mathbf{r},s)}{\partial s}=\frac{a^2}{6}\nabla^2q(\mathbf{r},s)-\delta_{i_+,s}w_{i_+}(\mathbf{r})q(\mathbf{r},s) \tag{5}$$

where $q(\mathbf{r},s)$ refers to either $q_+(\mathbf{r},s)$ or $q'_+(\mathbf{r},s)$, a is the size of the segment, $\delta_{i_+,s}$ is a Kronecker delta that equals to one if the segment-ranking number s of the cation is of type $i_+\in\{A,P\}$ and zero otherwise. Equation 5 is solved numerically subject to the initial and boundary conditions of the system. Since the open-end of the arm is occupied by an uncharged segment A and the center of the tetramer by the charged segment P, the initial condition at the open-end is $q_+(\mathbf{r},s_0)=\exp(-w_A(\mathbf{r}))$, whereas the initial condition at the center is $q'_+(\mathbf{r},s_0)=[q_+(\mathbf{r},s_{n_A})]^3$. The volume fraction $\varphi_{i_+}(\mathbf{r})$ of segment-i_+ in the cation is calculated from the convolution of $q_+(\mathbf{r},s)$ and its complementary value $q'_+(\mathbf{r},s)$,

$$\varphi_{i_+}(\mathbf{r})=\frac{Vf_+}{N_+Q_+}\int_0^{N_+}\delta_{i_+,s}q_+(\mathbf{r},s)q'_+(\mathbf{r},s)ds \tag{6}$$

in which $Q_+=\int q_+(\mathbf{r},s)q'_+(\mathbf{r},s)d\mathbf{r}$ is the partition function of the cation, which is independent to the segment-ranking number.

For the anion, the volume fraction of segment-i_-, where $i_- \in \{B, N\}$, is calculated in a similar manner as its cation counterpart. The corresponding diffusion equation for the chain connectivity of segments in the anion is,

$$\frac{\partial q(\mathbf{r},s)}{\partial s} = \frac{a^2}{6}\nabla^2 q(\mathbf{r},s) - \delta_{i_-,s} w_{i_-}(\mathbf{r}) q(\mathbf{r},s) \tag{7}$$

where $q(\mathbf{r},s)$ now refers to either $q_-(\mathbf{r},s)$ or $q'_-(\mathbf{r},s)$, and $\delta_{i_-,s}$ equals to one if the segment-ranking number s of the anion is of type i_- and zero otherwise. The initial condition at the open-end becomes $q_-(\mathbf{r},s_0) = \exp(-w_B(\mathbf{r}))$, whereas the initial condition at the center is $q'_-(\mathbf{r},s_0) = [q_-(\mathbf{r},s_{n_B})]^3$. The segment volume fraction in anion $\varphi_{i_-}(\mathbf{r})$ now reads,

$$\varphi_{i_-}(\mathbf{r}) = \frac{Vf_-}{N_- Q_-}\int_0^{N_-} \delta_{i_-,s} q_-(\mathbf{r},s) q'_-(\mathbf{r},s) ds \tag{8}$$

where the partition function of the anion is $Q_- = \int q_-(\mathbf{r},s) q'_-(\mathbf{r},s) d\mathbf{r}$.
The free energy formulation in Equations 1-4 implies that the local volume fraction $\varphi(\mathbf{r})$ and the local mean-field potential $w(\mathbf{r})$ are not independent towards one another. However, in a thermodynamical equilibrium the relationship between these two order parameters can be written based on a so-called saddle-point approximation, i.e.,

$$\begin{aligned} w_i(\mathbf{r}) \quad = \quad & \sum_{j\in\{A,P,B,N\}, j\neq i} \chi_{ij}(\varphi_j(\mathbf{r}) - \varphi_j^b) + \chi_{iS}\int \delta(\mathbf{r}-\mathbf{r_S}) d\mathbf{r} \\ & + \lambda(\mathbf{r}) + e\nu_i\psi(\mathbf{r}) - \frac{1}{2}\epsilon_0(\epsilon_{r,i}(\mathbf{r}) - 1)|\nabla\psi(\mathbf{r})|^2 \end{aligned} \tag{9}$$

where the Flory-Huggins parameter χ_{ij} in the first term represents the magnitude of the mean-field interaction between segment-i and -j. A more positive χ_{ij} indicates a more repulsive interaction. The parameter φ_j^b is the volume fraction of segment-j in the bulk. The local electrostatic potential $\psi(\mathbf{r})$ in the fourth term is obtained from the Poisson law, $\epsilon_0\nabla\left(\epsilon_r(\mathbf{r})\nabla\psi(\mathbf{r})\right) = -\sum_i e\nu_i\varphi_i(\mathbf{r})$. The last term of Equation 9 is a contribution from the polarization charges.(Feynman et al., 1964) Here, the permittivity of RTIL is considered a function of the collective permittivity of its constituent segments.(Bohmer et al., 1990; Reis et al., 2009) The local relative permittivity of the system is thus calculated from a linear combination of the local composition of its components, i.e., $\epsilon_r(\mathbf{r}) = \sum_i \epsilon_{r,i}\varphi_i(\mathbf{r})$, where $i \in \{A, P, B, N, S\}$. This involves a heuristic approach to assign a specific value of the relative permittivity $\epsilon_{r,i}$ to each segment-i in the system under a constraint that the overall (bulk) relative permittivity of the RTIL still mimics experimental values.(Koeberg et al., 2007; Krossing et al., 2006)
A complete self-consistent mean-field (SCMF) calculation consists of the following four steps: (i) a set of initial potential of segments is randomly generated; (ii) the corresponding volume fraction of all segments are obtained from Equations (6) and (8) after solving the chain propagators in Equations (5) and (7) by using the Scheutjens-Fleer scheme;(Scheutjens & Fleer, 1979; 1980) (iii) the Poisson equation is used to calculate the value of local electrostatic potential; (iv) a new set of segment potentials is calculated from Equation 9. Steps (i)-(iv) are then repeated until the difference between the volume fraction from the previous two iterations at any point $\mathbf{r}$ is less than 10^{-7}, which indicates that the free energy is extremized and the order parameters are self-consistent. Multiple independent calculations were performed with random initial segment potentials to ensure the results satisfy the ergodicity condition.

3. EDL structure and capacitance in RTILs

To study the shape of EDL capacitance curve for RTIL with the same ion size and without non-electrostatic (specific) affinity towards the electrode's surface, a series of SCMF calculation is performed using a tetrameric model of cation and anion (cf. Fig. 1) with $n_A = n_B = 4$.[1] For simplicity, the volume fraction of ions is assumed to vary only in the direction perpendicular to the electrode's surface. This means that the volume fraction of ions are homogeneous throughout each plane parallel to the surface. The size of all segments are set equal to 3 Å, which is of a similar order of magnitude to an ethyl chain or a heterocylic polar group in typical RTILs, such as pyrrolidinium and imidazolium rings. The system size is chosen large enough such that the bulk properties are reached within the boundaries of the modelled system. The relative permittivity of segments and electrode's surface used in the calculation are $\epsilon_{r,A} = \epsilon_{r,B} = 10$, $\epsilon_{r,P} = \epsilon_{r,N} = 30$, and $\epsilon_{r,S} = 10$. These values are chosen such that the relative permittivity of the modelled RTIL in the bulk is similar to the real value, which is $\sim$ 11-12.(Koeberg et al., 2007; Krossing et al., 2006) The interaction parameter $\chi_{AB} = 1$ is used to represent an adequate repulsion between uncharged segment-A of cation and -B of anion.

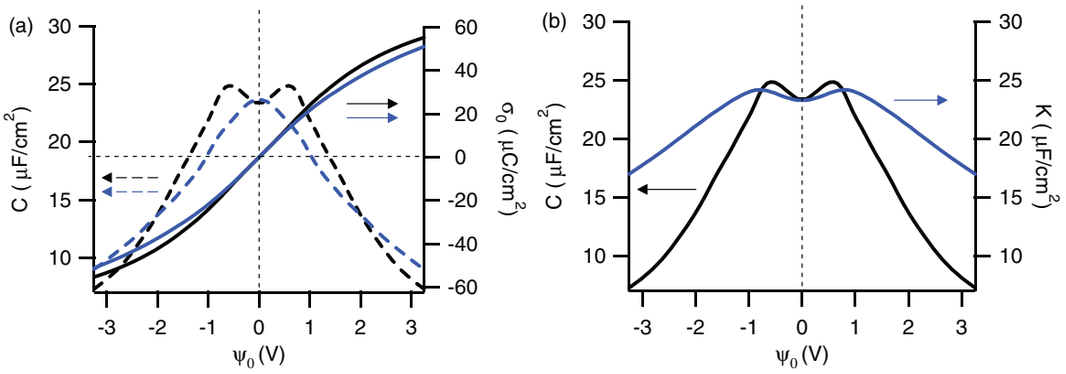

Fig. 2. (a) Full line: plot of the surface charge (σ_0) as a function of the surface potential (ψ_0). Dashed line: plot of the corresponding differential capacitance curve (C). The black and the blue curves are generated with and without the use of an effective dielectric constant, respectively. (b) Plot of the differential capacitance curve (black) compared to the integral capacitance curve (blue).

The surface charge (σ_0) and the differential capacitance (C) are plotted as functions of the surface potential (ψ_0) in Fig. 2a. For comparison, the differential and integral capacitance curves are depicted together in Fig. 2b. The differential capacitance is calculated from the first derivative of the surface charge (σ_0) with respect to ψ_0, i.e., $C = \frac{\partial \sigma_0}{\partial \psi_0}$. The integral capacitance is obtained by dividing the surface charge with the surface potential, i.e., $K = \frac{\sigma_0}{\psi_0}$. Note that the value of differential capacitance based on an equilibrium model like SCMFT can only be related to that obtained from impedance spectroscopy at very low frequencies. Figure 2a shows that the bell-shaped differential capacitance curve is obtained when a uniform dielectric constant of segments is used. In this case, the value used is $\epsilon_{r,A} = \epsilon_{r,P} = \epsilon_{r,B} = \epsilon_{r,N} = 11$. When the effective dielectric constant is taken into account, the differential capacitance curve has a camel-like shape with two maxima. This is also the case for the integral capacitance (cf.

[1] The detailed version of this part can be found in (Lauw et al., 2009).

Fig. 2b) although compared to the differential capacitance the maxima are reached at slightly larger potential values and the decrease in capacitance at both potential wings is less steep. The curve of surface charge in Fig. 2a comprises two regimes, namely a quasi-linear regime at low electrostatic potentials (-0.63 V $< \psi_0 <$ 0.63 V) and a non-linear regime at high potentials ($|\psi_0| >$ 0.63 V). The term quasi-linear is used here since within this region the relationship between the surface charge and the surface potential appears to be linear, yet from the capacitance curve it is clear that the surface charge has a point of inflection at the pzc, which in this case is located at $\psi_0 = 0$. In the quasi-linear regime, the electrode's surface is still not yet fully saturated by counterions, whereas the counterions saturate the electrode's surface and accumulate further away towards the bulk in the non-linear regime, as illustrated by the set of volume fraction profile of cation and anion in Fig. 3. Note that the fluctuation of electrostatic potential at the interface at various applied potentials (cf. Fig. 4a) indicates that the charge overscreening takes place in both quasi-linear and non-linear regimes.

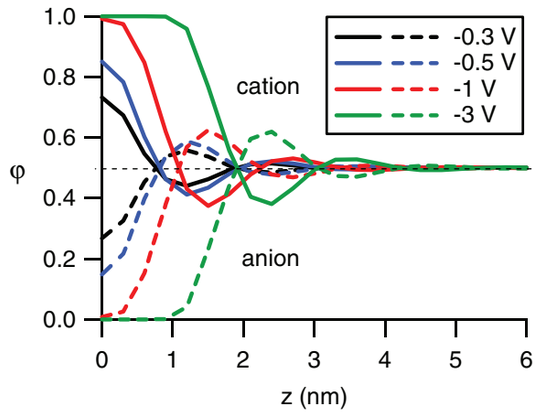

Fig. 3. Profile of the volume fraction of cation and anion at the interface at different surface potential values. The abscissa z indicates the distance from the electrode's surface.

Figure 2 shows that the capacitance curve has a camel-like shape, which is symmetric with respect to the pzc and reaches maxima at $|\psi_0| = 0.63$ V. It is worth noting that the camel-shaped capacitance curve is not unique to RTILs. It was first observed decades ago in the study of aqueous solutions of NaI, NaF, KPF_6, and KBF_4 on Au or Ag electrodes, where specific adsorptions occur.(Clavilier & Huong, 1977; Grahame, 1947; Hamelin & Stoicoviciu, 1987; Valette, 1981) In aqueous electrolytes, the hump on the capacitance curves is typically a direct consequence of non-homogeneous polarization in the EDL.(MacDonald, 1954; MacDonald & Barlow Jr., 1962; Parsons, 1961) Arguably, the primary cause for such a capacitance curve in RTILs may be different. The camel-shaped capacitance curves can be obtained using theoretical models, in which ions are considered to have finite sizes. This approach goes beyond typical Poisson-Boltzmann approximation which assumes ions as point charges. In SCMFT, the excluded volume effect is incorporated by modelling ions as segmented dendrimers with a sufficient repulsion between uncharged segments A and B in the branches of each cation and anion. It is apparent from Figure 2a that the excluded volume is not the only effect causing the camel-shaped capacitance curve. By considering the effective dielectric constant of RTILs as a function of the local segment density, it is shown that the polarizability of ions at the interface turns out to be another key factor. The camel-shaped capacitance curve can be analysed based on the potential-dependence of the structure of RTILs at the interface. This structure-property relationship is elaborated further as follows:

a) Within the quasi-linear regime ($|\psi_0| < 0.63$ V), the capacitance increases with the surface potential. Following the trend of the volume fraction profiles of ions shown in Fig. 3, one can conclude that at the points where the capacitance reaches its maximum values ($|\psi_0| = 0.63$ V), the electrode's surface is saturated with counterions. Between these two points, some coions can still be found at the surface. The alternating layer of ions can be considered as a series of capacitors with the corresponding capacitance value is obtained from $1/C = \sum_l 1/C_l$, where C_l is the capacitance of layer-l. Based on this representative formula, the capacitance of the EDL in RTILs is determined by a non-trivial balance between the thinning/thickenning of each layer and the decreasing/increasing polarization. A higher capacitance value can be a result of thinner layers and/or a larger interfacial polarization. Results from SCMFT indicate that the thickness and periodicity of each alternate layer throughout the quasi-linear regime is relatively the same, whereas the local dielectric constants ϵ_r differ following the local distribution of molecular segments (cf. Fig. 4b for the case of $\psi_0 = -0.3$ V and -0.5 V). Therefore, an increasing capacitance in the quasi-linear regime is likely to be driven by an increasing polarization of RTILs at the interface.

b) Within the non-linear regime ($|\psi_0| > 0.63$ V), the surface charge is less than a linear function of the surface potential and the capacitance decreases with increasing surface potential. The physical interpretation is that the energy needed to bring one counterion from the bulk to the surface increases more than linearly with an increasing surface charge. In this regime, the interface is already saturated with counterions such that the EDL thickness grows with an increasing surface potential, as shown in Fig. 3 for $\psi_0 = -1$ V and -3 V. Moreover, the charged segment of the counterions is primarily located at the electrode's surface, causing a higher dielectric constant value there (cf. Fig. 4b). A thicker EDL overcomes the effect of an increasing polarization at the interface to lower the capacitance. The scaling of the capacitance in the non-linear regime is $C \propto |\psi_0|^{-0.82}$. As a comparison, the scaling for the bell-shaped capacitance curve is $C \propto |\psi_0|^{-0.60}$, which indicates that the effective dielectric constant plays an important role in determining the scale of the capacitance at the electrostatic potential wings.

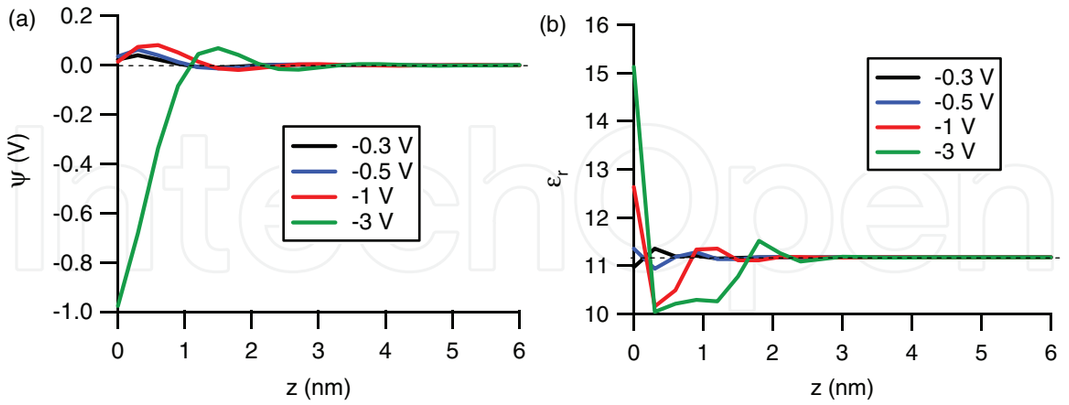

Fig. 4. (a) Profile of the diffuse electrostatic potential at the interface at different surface potentials. (b) Profile of the corresponding local dielectric constant (ϵ_r).

In aqueous electrolyte solutions, an increasingly charged electrode leads to a more effective screening of the electrostatic potential. The screening effect intensifies as the interface is more densely populated by counterions which replace electroneutral water molecules. As a result, the curvature of $\sigma_0(\psi_0)$ goes beyond linear. At a first glance, the overall capacitance

curve of the EDL in aqueous electrolytes seems to differ from that in RTILs. The capacitance curve in aqueous electrolytes usually reaches a minimum at pzc and increases monotonically with surface potential, whereas the capacitance curve in RTILs has a camel-like shape. Nevertheless, under similar premises both curves would have the same camel-like shape if similar potential limits could be attained. This means that the maxima of the capacitance curve in aqueous electrolytes occur at potentials beyond the electrochemical window of water, such that one never observed this camel-shaped capacitance curve in reality.
The effects of different ion-size and specific adsorption of ions to the EDL capacitance in RTILs are discussed in the following two sections. The complete version of these sections can be found in (Lauw et al., 2010).

3.1 Effect of different ion-size

Results from the SCMFT described above were based on a uniform dendrimeric model of cation and anion, without taking into account ions of different size. In most RTILs, the anions are relatively smaller than the cations. Here, three size ratios of cation and anion are used to study the effect of ion-size on capacitance. This is achieved by varying the length of each arm in the anion while keeping the cation size the same. Three ratios of the arm's length used in this study are $n_A : n_B$ = 4:4, 4:3, and 4:2. The differential capacitance curve for the three size ratios of cation and anion are plotted in Fig. 5a. Each differential capacitance curve has a camel-shaped feature, which is symmetric for RTIL with the same ion-size (n_A:n_B = 4:4) and asymmetric for ions with unequal size (n_A:n_B = 4:3 and 4:2). The asymmetry is caused by the deviation in the corresponding $\sigma_0(\psi_0)$ curves at positive applied potentials, as shown in Fig. 5a. The comparison between the differential and integral capacitance curves for unequal ion-size is shown in Fig. 5b. Although in principle the shape of both curves are similar, the integral capacitance curve is non-continuous at $\psi_0 = 0$.

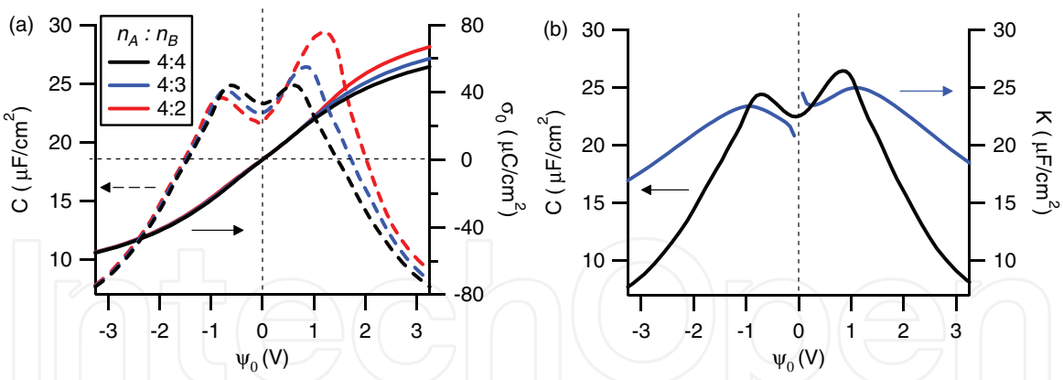

Fig. 5. (a) Plot of the differential capacitance (left) and the corresponding surface charge (right) as functions of the surface potential of the modelled RTIL with different ratios of n_A:n_B, as indicated. (b) Plot of the differential capacitance curve (black) and the integral capacitance curve (blue) for the case of n_A:n_B = 4:3.

It is known that the minimum differential capacitance is typically reached at the pzc, where the electrode's surface charge is practically zero. As described in the previous section, the quasi-linear regime is located around the pzc. For the modelled RTIL with n_A:n_B = 4:4, this regime is located within -0.63 V $< \psi_0 <$ 0.63 V. It expands further for RTILs with unequal ion-size, i.e., -0.73 V $< \psi_0 <$ 0.83 V for n_A:n_B = 4:3, and -0.83 V $< \psi_0 <$ 1.19 V for n_A:n_B = 4:2. The complete list of the pzc, location of both maximum potential values ($\psi_0^{\max -}$

and $\psi_0^{\max_+}$), and the extrema of the capacitance curves (C_{pzc}, $C_{\max_-}$, and $C_{\max_+}$) are shown in Table 1. Here, the indices $\max_-$ and $\max_+$ indicate values at the maximum capacitance on the left-hand and right-hand sides of pzc, respectively. Parameters α_- and α_+ are the exponents from the scaling of the capacitance with respect to each surface potential wing in the non-linear regime, i.e., $C \propto |\psi_0|^{\alpha_-}$ for $\psi_0 < \psi_0^{\max_-}$ and $C \propto |\psi_0|^{\alpha_+}$ for $\psi_0 > \psi_0^{\max_+}$.

n_A:n_B	pzc (mV)	$\psi_0^{\max_-}$ (V)	$\psi_0^{\max_+}$ (V)	C_{pzc} (μF/cm^2)	$C_{\max_-}$ (μF/cm^2)	$C_{\max_+}$ (μF/cm^2)	α_-	α_+
4:4	0	−0.63	0.63	23.30	24.85	24.85	−0.82	−0.82
4:3	−6	−0.73	0.83	22.46	24.40	26.42	−0.82	−1.04
4:2	−12	−0.83	1.19	21.60	23.80	29.39	−0.82	−1.32

Table 1. List of critical values and scaling parameters for differential capacitance curves in Fig. 5a.

Figure 5 indicates that the impact of smaller anions on capacitance becomes more significant with an increasingly positive potential, as also shown by a more prominent deviation of $\sigma_0(\psi_0)$ there. It is also apparent that the shape of capacitance curve is strongly influenced by the the size of counterion, whereas the effect of coion size seems to be limited. In general, smaller ions have a larger packing density and screen electrostatic potential more effectively. For smaller anions, these two factors cause a positive shift in $\psi_0^{\max_+}$ and, to a lesser extent, a negative shift in $\psi_0^{\max_-}$. The positive shift is needed to accommodate the increasing number of anions required to saturate the Helmholtz layer, whereas the negative shift would counter the increase in screening effect of anions at the interface. A slightly negative pzc found for smaller anions is a result of the size mismatch between anion and cation, which leads to a population inbalance of ions near the surface. At zero surface charge (pzc), this inbalance results in a slightly non-zero (negative) excess charge in the Helmholtz layer, which is then overcompensated by opposite charges in subsequent layers. Besides causing the shift in critical potentials, less bulky anions raise the capacitance value at $\psi_0 > 0.63$ V and lower it in -0.83 V $< \psi_0 < 0.63$ V. The former occurs due to the formation of more compact alternate layers by smaller anions, as illustrated in Fig. 6a; the latter is a result of less polarized alternate layers, as the screening effect of smaller anions dampens the potential field more effectively. To illustrate the last point, the mole fraction profile of ions at this region ($\psi_0 = -0.6$ V) is shown in Fig. 6b. The changes in capacitance described here are in a good agreement with those from spectroscopic study of RTILs composed of imidazolium-based cations and Cl or BF_4 anions on glassy carbon, gold, or mercury electrodes.(Alam et al., 2007; 2008; Lockett et al., 2008)

The scaling of differential capacitance in RTILs with applied potential at both potential wings is a good indication of the extent of the compression of ions due to a high electrostatic field (electrostriction) in the EDL. For the case of $n_A : n_B = 4{:}4$, the scale is identical in the first non-linear regime ($\psi_0 < \psi_0^{\max_-}$) and the second non-linear regime ($\psi_0 > \psi_0^{\max_+}$), which is $C \propto |\psi_0|^{-0.82}$. For asymmetric capacitance curves, this scale persists in the first non-linear regime and becoming more pronounced in the second regime, in which the scaling is $C \propto |\psi_0|^{-1.04}$ for $n_A : n_B = 4{:}3$, and $C \propto |\psi_0|^{-1.32}$ for $n_A : n_B = 4{:}2$. Each scaling exponent corresponds to the change in thickness of alternate layers with electrostatic potential since the capacitance in the non-linear regime is mainly determined by the size of these layers. In principle, less bulky anions are geometrically more susceptible to variation in potential field by forming thicker (thinner) alternate layers at a more (less) positive applied potential. This

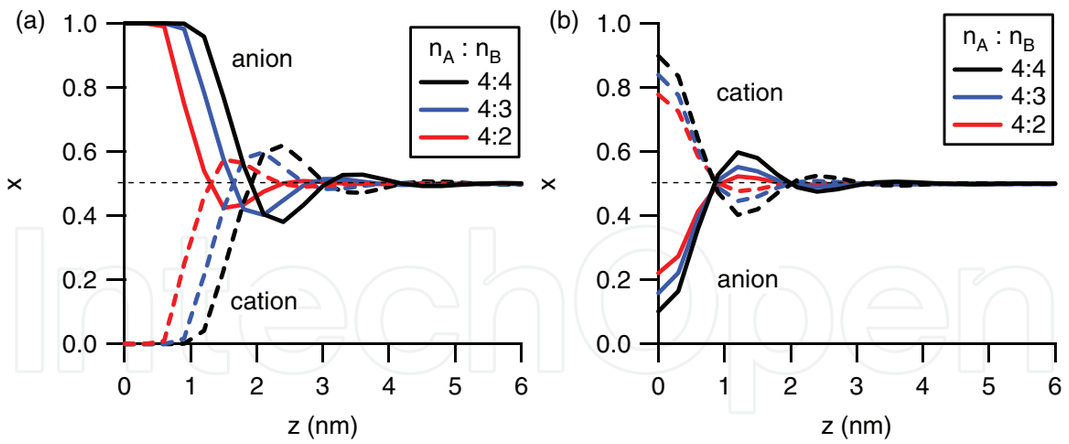

Fig. 6. Profile of the mole fraction (x) of cation and anion at the interface with different ratios of n_A:n_B at $\psi_0 = 3$ V (a), and $\psi_0 = -0.6$ V (b).

explains a more rapid decay of the capacitance in the second non-linear regime for smaller anions. It is interesting to note that all scaling exponents obtained here are considerably less than -0.5, which is the value predicted analytically based on the Poisson-Fermi distribution of spherical ions at a charged interface.(Kornyshev, 2007) This discrepancy is originated from different underlying assumptions in the analytical and SCMFT model. The analytical model incorporated the excluded volume by introducing a fixed lattice saturation parameter into the Boltzmann distribution of ions. In SCMFT, the lattice saturation parameter would not be homogeneous throughout the system since the ions are modelled as flexible chain molecules and their compression or relaxation within the EDL would depend on the local electrostatic potential field. This makes the EDL structure more responsive to the applied potential, which results in a more rapid decay of $C(\psi_0)$ than analytically predicted.

3.2 Effect of specific adsorption

Asymmetric capacitance curves in RTILs do not only occur when the corresponding ions have different size. They also occur for same-size ions with different specific affinity towards the electrode's surface. In aqueous electrolytes, specific adsorption is strongly related to the solvation shell of ions. A steric hindrance provided by a thick solvation shell prevents the ions from forming chemical bonds with the surface. For ions with thin-enough solvation shells, the solvent molecules would be removed from the surface to accommodate adsorption of more ions. This eventually leads to a redistribution of local charges on the surface, changes the surface dipole, and induces a partial charge transfer.(Lipowski et al., 1998; Lorenz & Salie, 1977; Magnussen, 2002) In the absence of any solvation shells surrounding RTILs, the specific adsorption of ions would arguably occur more strongly than in aqueous electrolytes.(Aliaga & Baldelli, 2006; Gale & Osteryoung, 1980) An example of specific adsorption in pure RTILs has been reported for 1-butyl-3-methylimidazolium dicyanamide RTIL on Pt-electrode.(Aliaga & Baldelli, 2006)

To study the effect of specific adsorption to the capacitance in RTILs, the affinity of anion towards the electrode's surface is systematically varied, while the size of the cation and anion is kept the same at $n_A : n_B = 4{:}4$. Three different sets of interaction parameters used here are $\chi_{BS} = \chi_{NS} = 0$, -1, and -2. The more negative interaction parameter indicates a stronger specific affinity of anion towards the surface. The values of interaction parameter used here are within the typical limit of adsorption energy due to specific interactions, which

is in the order of few k_BT for each adsorbed ion.(Lamperski, 1997; Lyklema, 1995; Nikitas, 1994; Parsons, 1955)

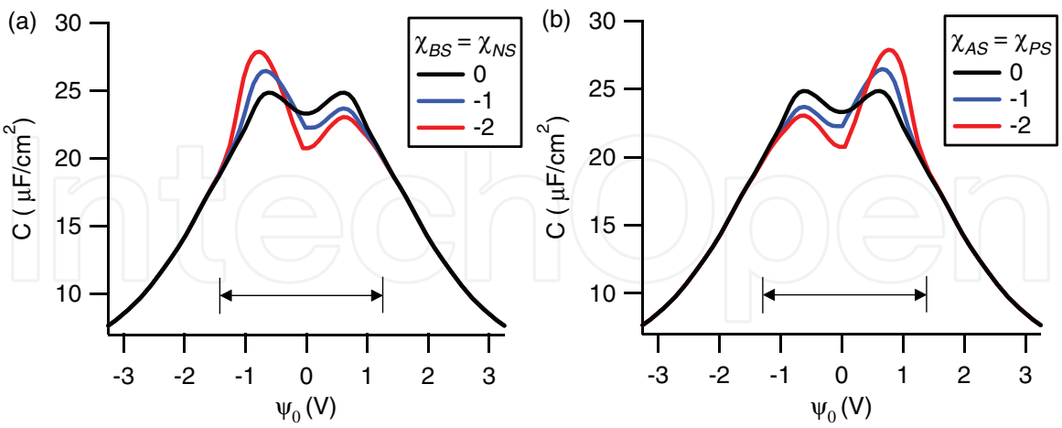

Fig. 7. (a) The differential capacitance curves of the modelled RTIL with n_A:n_B = 4:4 and $\chi_{BS} = \chi_{NS} = 0, -1$, and -2. (b) Similar curves with $\chi_{AS} = \chi_{PS} = 0, -1$, and -2. In both cases, the impact of specific adsorption is limited in the ψ_0-zone marked by the arrow. It is apparent that the curve is asymmetric with respect to the pzc when the specific adsorption is present.

The differential capacitance curves of the aforementioned system are plotted in Fig. 7a. For comparison, a series of differential capacitance curves for the case of specific adsorption of cation is shown in Fig. 7b. These curves are understandably the mirror image of those obtained when the specific adsorption of anion is present. The critical values for the capacitance curves in Fig. 7a are listed in Table 2. It appears that a stronger specific adsorption of anion increases the capacitance value at -1.2 V $< \psi_0 < -0.3$ V and decreases it at -0.3 V $< \psi_0 < 1.2$ V. The trend is reversed when the specific adsorption of cation is stronger (cf. Fig. 7b). The physical interpretation of these trends is that the amount of energy to bring one counterion from the bulk to the surface would be either reduced by the presence of specifically adsorbed coion, or increased when some counterion is already specifically adsorbed on the surface.

$\chi_{BS} = \chi_{NS}$	pzc (mV)	$\psi_0^{\max_-}$ (V)	$\psi_0^{\max_+}$ (V)	C_{pzc} (μF/cm^2)	$C_{\max_-}$ (μF/cm^2)	$C_{\max_+}$ (μF/cm^2)
0	0	-0.63	0.63	23.30	24.85	24.85
-1	-52	-0.66	0.61	22.27	26.45	23.67
-2	-95	-0.77	0.60	20.76	27.86	23.03

Table 2. List of critical values for differential capacitance curves in Fig. 7a.

The impact of specific adsorption is typically confined within a limited range of applied potential from the pzc.(Graves, 1970) This ψ_0-zone is located in -1.2 V $< \psi_0 < 1.2$ V for capacitance curves depicted in Fig. 7. As discussed above, specifically adsorbed ions tend to increase the gradient of $C(\psi_0)$ in the ψ_0-zone. Such a steep capacitance curve is typically caused by partial charge transfers at a non-ideally polarized surface, which can be induced by specifically adsorbed ions.(Lipowski et al., 1998; Lorenz & Salie, 1977; Magnussen, 2002; Parsons, 1981) Beyond the ψ_0-zone, the long-range electrostatic interaction overcomes the short-range effect of specific adsorption to diminish the amount of adsorbed anion on the

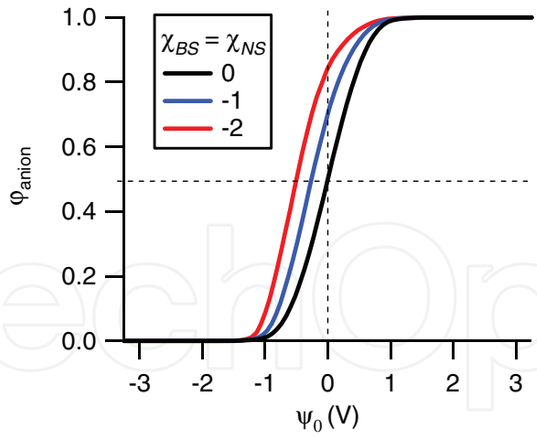

Fig. 8. Plot of the volume fraction of anion on the electrode's surface (φ_{anion}) as a function of applied potential. There is a significant amount of anion on the electrode's surface even at negative potentials due to the specific adsorption.

surface (φ_{anion}) at negative potential, as shown in Fig. 8. There are two additional trends observed by increasing the specific affinity of anion. Firstly, the φ_{anion} curve shifts to the left, indicating an increasing presence of anion on a negatively charged surface. Secondly, the pzc and both saturation limits ($\psi_0^{\max_-}$ and $\psi_0^{\max_+}$) shift to more negative values since, in principle, a more negative surface is needed to counter the increasing amount of specifically adsorbed anion.

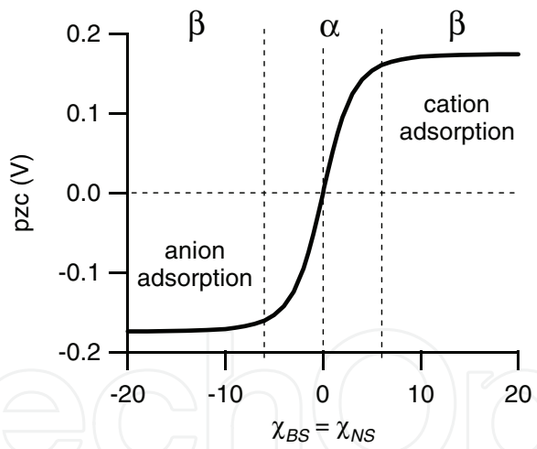

Fig. 9. Plot of the pzc as a function of the strength of specific adsorption of ion. For $\chi_{BS} = \chi_{NS} < 0$, the anion is adsorbed specifically to the surface, whereas for $\chi_{BS} = \chi_{NS} > 0$, the cation is specifically adsorbed.

The pzc is a robust parameter to detect the existence of specific adsorption in RTILs. The shift of pzc due to specific adsorption is relatively larger than that for unequal ion-size (cf. Tables 1 and 2). The relationship between the pzc and the strength of specific adsorption is shown in Fig. 9. The pzc varies steadily in the α-zone ($|\chi_{BS}| = |\chi_{NS}| < 6$) and goes to asymptotic values at the limit of extreme adsorption in the β-zone ($|\chi_{BS}| = |\chi_{NS}| > 6$). The gradient of the pzc curve in the α-zone is $\sim 2k_BT$ per ion for each unit of interaction parameter ($\chi_{BS} = \chi_{NS}$). In the β-zone, the gradient is close to zero, indicating the saturation of Helmholtz layer by specifically adsorbed ions.

4. Concluding remarks

The interfacial structure and capacitance in RTILs are studied by the SCMFT. Each ion is modelled as a tetramer composed of polar and apolar segments. The results show that the alternating layer of ions is formed at charged interfaces and the corresponding capacitance curve has a camel-shaped feature. The latter is caused by a combination of the excluded volume and ion polarizability effects in the EDL. The introduction of unequal ion-size leads to asymmetric capacitance curves. The shape of these curves is strongly determined by the size of counterion and only weakly influenced by coion size. In general, smaller ions have a higher packing density and screen the electrostatic potential more effectively. These two factors cause a shift in critical values of the capacitance curves. The presence of a specific affinity of ions towards the electrode's surface also leads to asymmetric capacitance curves. The impact occurs only within a limited range of applied potential from the pzc. Besides changing the capacitance values, specifically adsorbed ions shift the pzc and both saturation limits of the capacitance curves to one direction, depending on the type of their charge and the strength of specific adsorption.

The change in the pzc can be used as a qualitative tool to predict, e.g., the type of RTIL-metal species specifically adsorbed on the electrode's surface during metal electrodeposition, provided that each species has a distinct size but similar affinity towards the surface. The trends in capacitance curve and pzc presented in this study are generally useful to assist in the choice of RTILs for specific electrochemical applications, and in the design of new RTILs with tailored electrochemical properties.

5. Acknowledgement

The authors would like to thank Bart Follink, Theo Rodopoulos, Mike Horne (CSIRO), and Andy Nelson (ANSTO) for helpful discussion in this work.

6. References

Alam, M.T.; Islam, M.M.; Okajima, T. & Ohsaka, T. (2007). Measurements of differential capacitance at mercury/room-temperature ionic liquids interfaces. *Journal of Physical Chemistry C*, Vol. 111, 18326-18333.

Alam, M. T.; Islam, M.M.; Okajima, T. & Ohsaka, T. (2008). Capacitance measurements in a series of room-temperature ionic liquids at glassy carbon and gold electrode interfaces. *Journal of Physical Chemistry C*, Vol. 112, 16600-16608.

Aliaga, C. & Baldelli, S. (2006). Sum frequency generation spectroscopy and double-layer capacitance studies of the 1-butyl-3-methylimidazolium dicyanamide-platinum interface. *Journal of Physical Chemistry B*, Vol. 110, 18481-18491.

Armand, M.; Endres, F.; MacFarlane, D.R.; Ohno, H. & Scrosati, B. (2009). Ionic-liquid materials for the electrochemical challenges of the future. *Nature Materials*, Vol. 8, 621-629.

Atkin, R. & Warr, G.G. (2007). Structure in confined room-temperature ionic liquids. *Journal of Physical Chemistry C*, Vol. 111, 5162-5168.

Atkin, R.; El Abedin, S.Z.; Hayes, R.; Gasparotto, L.H.S.; Borisenko, N. & Endres, F. (2009). AFM and STM studies on the surface interaction of [BMP]TFSA and [EMIm]TFSA ionic liquids with Au(111). *Journal of Physical Chemistry C*, Vol. 113, 13266-13272.

Baldelli, S. (2008). Surface structure at the ionic liquid-electrified metal interface. *Accounts of Chemical Research*, Vol. 41, 421-431.

Bazant, M.Z.; Kilic, M.S.; Storey, B.D. & Ajdari, A. (2009). Nonlinear electrokinetics at large voltages. *New Journal of Physics*, Vol. 11, 075016.

Bikerman, J.J. (1942). Structure and capacity of electrical double layer. *Philosophical Magazine*, Vol. 33, 384-397.

Bohmer, M.R.; Evers, O.A. & Scheutjens, J.M.H.M. (1990). Weak polyelectrolytes between two surfaces: Adsorption and stabilization. *Macromolecules*, Vol. 23, 2288-2301.

Chmiola, J.; Largeot, C.; Taberna, P.L.; Simon, P. & Gogotsi, Y. (2008). Desolvation of ions in subnanometer pores and its effect on capacitance and double-layer theory. *Angewandte Chemie International Edition*, Vol. 47, 3392-3395.

Claessens, M.M.A.E.; van Oort, B.F.; Leermakers, F.A.M.; Hoekstra, F.A. & Cohen Stuart, M.A. (2004). Charged lipid vesicles: Effects of salts on bending rigidity, stability, and size. *Biophysical Journal*, Vol. 87, 3882-3893.

Clavilier, J. & Huong, C.N.V. (1977). Etude de l'interface de l'or polycristallin au contact de solutions aqueuses de perchlorate de potassium et d'acide perchlorique. *Journal of Electroanalytical Chemistry*, Vol. 80, 101-114.

Edwards, S.F. (1965). The statistical mechanics of polymers with excluded volume. *Proceedings of the Physical Society of London*, Vol. 85, 613-624.

Endres, F.; MacFarlane, D. & Abbott, A. (2008). *Electrodeposition from ionic liquids*, Wiley-VCH, Weinheim, Germany.

Fedorov, M.V. & Kornyshev, A.A. (2008). Towards understanding the structure and capacitance of electrical double layer in ionic liquids. *Electrochimica Acta*, Vol. 53, 6835-6840.

Feng, G.; Zhang, J.S. & Qiao, R. (2009). Microstructure and capacitance of the electrical double layers at the interface of ionic liquids and planar electrodes. *Journal of Physical Chemistry C*, Vol. 113, 4549-4559.

Feynman, R.P.; Leighton, R.B. & Sands, M. (1964). *Lectures on Physics II*, Addison-Wesley Publishing Company, Reading, MA.

Fleer, G.J.; Cohen Stuart, M.A.; Scheutjens, J.M.H.M.; Cosgrove, T. & Vincent, B. (1993). *Polymers at interface*, Chapman and Hall, London, UK.

Flory, P.J. (1953). *Principles of Polymer Chemistry*, Cornell University Press, New York.

Freise V. (1952). Zur Theorie der diffusen Doppelschicht. *Zeitschrift fur Elektrochemie*, Vol. 56, 822-827.

Gale, R.J. & Osteryoung, R.A. (1980). The electrical double layer at mercury in room temperature aluminum chloride: 1-butylpyridinium chloride ionic liquids. *Electrochimica Acta*, Vol. 25, 1527-1529.

Grahame, D.C. (1947). The electrical double layer and the theory of electrocapillarity. *Chemical Reviews*, Vol. 41, 441-501.

Graves, A.D. (1970). The electrical double layer in molten salts. Part 1. The potential of zero charge. *Journal of Electroanalytical Chemistry* Vol. 25, 349-356.

Hamelin, A. & Stoicoviciu, L. (1987). Study of gold low index faces in KPF_6 solutions. Part I. Experimental behaviour and determination of the points of zero charge. *Journal of Electroanalytical Chemistry*, Vol. 234, 93-105.

Horn, R.G.; Evans, D.F. & Ninham, B.W. (1988). Double-layer and solvation forces measured in a molten salt and its mixtures with water. *Journal of Physical Chemistry*, Vol. 92, 3531-3537.

James, R.O. & Healy, T.W. (1972). Adsorption of hydrolyzable metal ions at the oxide-water interface. III. A thermodynamic model of adsorption. *Journal of Colloid and Interface Science*, Vol. 40, 65-81.

Kilic M.S.; Bazant, M.Z. & Ajdari, A. (2007). Steric effects in the dynamics of electrolytes at large applied voltages. I. Double-layer charging. *Physical Review E*, Vol. 75, 021502.

Koeberg, M.; Wu, C.C.; Kim, D. & Bonn, M. (2007). THz dielectric relaxation of ionic liquid:water mixtures. *Chemical Physics Letters*, Vol. 439, 60-64.

Kornyshev, A.A. (2007). Double-layer in ionic liquids: Paradigm change? *Journal of Physical Chemistry B*, Vol. 111, 5545-5557.

Krossing, I.; Slattery, J.M.; Daguenet, C.; Dyson, P.J.; Oleinikova, A. & Weingartner, H. (2006). Why are ionic liquids liquid? A simple explanation based on lattice and solvation energies. *Journal of American Chemical Society*, Vol. 128, 13427-13434.

Lamperski, S. (1997). Molecular model for anion adsorption from electrolyte of constant ionic strength. *Journal of Electroanalytical Chemistry*, Vol. 437, 225-231.

Largeot, C.; Portet, C.; Chmiola, J.; Taberna, P.L.; Gogotsi, Y. & Simon, P. (2008). Relation between the ion size and pore size for an electric double-layer capacitor. *Journal of American Chemical Society*, Vol. 130, 2730-2731.

Lauw, Y.; Kovalenko, A. & Stepanova, M. (2008). Phase behavior of amphiphilic lipid molecules at air-water interfaces: An off-lattice self-consistent-field modeling. *Journal of Physical Chemistry B*, Vol. 112, 2119-2127.

Lauw, Y. (2009). Equilibrium morphologies of nonionic lipid-nanoparticle mixtures in water: A self-consistent mean-field prediction. *Journal of Colloid and Interface Science*, Vol. 332, 491-496.

Lauw, Y.; Horne, M.D.; Rodopoulos, T. & Leermakers, F.A.M. (2009). Room-temperature ionic liquids: Excluded volume and ion polarizability effects in the electrical double-layer structure and capacitance. *Physical Review Letters*, Vol. 103, 117801.

Lauw, Y.; Horne, M.D.; Rodopoulos, T.; Nelson, A. & Leermakers, F.A.M. (2010). Electrical double-layer capacitance in room temperature ionic liquids: ion-size and specific adsorption effects. *Journal of Physical Chemistry B*, Vol. 114, 11149-11154.

Leermakers, F.A.M.; Rabinovich, A.L. & Balabaev, N.K. (2003). Self-consistent-field modeling of hydrated unsaturated lipid bilayers in the liquid-crystal phase and comparison to molecular dynamics simulations. *Physical Review E*, Vol. 67, 011910.

Leermakers, F.A.M.; Eriksson, J.C. & Lyklema, J. (2005). *Fundamentals of Interface and Colloid Science V, Chapter 4*, Elsevier, Amsterdam, The Netherlands.

Lipowski, J.; Shi, Z.; Chen, A.; Pettinger, B. & Bilger, C. (1998). Ionic adsorption at the Au(ll1) electrode. *Electrochimica Acta*, Vol. 43, 2875-2888.

Lockett, V.; Sedev, R.; Ralston, J.; Horne, M.D. & Rodopoulos, T. (2008). Differential capacitance of the electrical double layer in imidazolium-based ionic liquids: Influence of potential, cation size, and temperature. *Journal of Physical Chemistry C*, Vol. 112, 7486-7495.

Lorenz, W. & Salie, G.G. (1977). Partial charge transfer reactions in electrochemical kinetics. Review on the theory of measuring methods for electrode processes with adsorbed intermediates. *Journal of Electroanalytical Chemistry*, Vol. 80, 1-56.

Lyklema, J. (1995). *Fundamentals of Interface and Colloid Science II, Chapter 3*, Elsevier, Amsterdam, The Netherlands.

MacDonald, J.R. (1954). Theory of the differential capacitance of the double layer in unadsorbed electrolytes. *Journal of Chemical Physics*, Vol. 22, 1857-1866.

MacDonald, J.R. & Barlow Jr., C.A. (1962). Theory of double-layer differential capacitance in electrolytes. *Journal of Chemical Physics*, Vol. 36, 3062-3080.

Magnussen, O.M. (2002). Ordered anion adlayers on metal electrode surfaces. *Chemical Reviews*, Vol. 102, 679-725.

Matsen, M.W. (1995). Phase behavior of block copolymer/homopolymer blends. *Macromolecules*, Vol. 28, 5765-5773.

Mezger, M.; Schroder, H.; Reichert, H.; Schramm, S.; Okasinski, J.S.; Schoder, S.; Honkimaki, V.; Deutsch, M.; Ocko, B.M.; Ralston, J.; Rohwerder, M.; Stratmann, M. & Dosch, H. (2008). Molecular layering of fluorinated ionic liquids at a charged sapphire (0001) surface. *Science*, Vol. 322, 424-428.

Mezger, M.; Schramm, S.; Schroder, H.; Reichert, H.; Deutsch, M.; De Souza, E.J.; Okasinski, J.S.; Ocko, B.M.; Honkimaki, V. & Dosch, H. (2009). Layering of $[BMIM]^{+}$-based ionic liquids at a charged sapphire interface. *Journal of Chemical Physics*, Vol. 131, 094701.

Nikitas, P. (1994). A new approach to development of ionic isotherms of specific adsorption in the electrical double layer. *Journal of Physical Chemistry B*, Vol. 98, 6577-6585.

Ohno, H. (2005). *Electrochemical aspects of ionic liquids*, John Wiley & Sons, Inc., Hoboken, NJ.

Oldham, K.B. (2008). A GouyŰChapmanŰStern model of the double layer at a (metal)/(ionic liquid) interface. *Journal of Electroanalytical Chemistry*, Vol. 613, 131-138.

Outhwaite, C.W.; Bhuiyan, L.B. & Levine, S. (1980). Theory of the electric double layer using a modified Poisson-Boltzmann equation. *Journal of Chemical Society - Faraday Transactions*, Vol. 76, 1388-1408.

Parsons, R. (1955). The specific adsorption of ions at the metal-electrolyte interphase. *Transactions of the Faraday Society*, Vol. 51, 1518-1529.

Parsons, R. (1961). *Advances in Electrochemistry and Electrochemical Engineering Volume I, Chapter 1*, Interscience Publishers, NY.

Parsons, R. (1981). The contribution to the capacity of an electrode from a species adsorbed with partial charge transfer. *Canadian Journal of Chemistry*, Vol. 59, 1898-1902.

Parsons, R. (1990). Electrical double layer: Recent experimental and theoretical developments. *Chemical Reviews*, Vol. 90, 813-826.

Reed, S.K.; Madden, P.A. & Papadopoulos A. (2008). Electrochemical charge transfer at a metallic electrode: A simulation study. *Journal of Chemical Physics*, Vol. 128, 124701.

Reis, J.C.R.; Iglesias, T.P.; Douheret, G. & Davis, M.I. (2009). The permittivity of thermodynamically ideal liquid mixtures and the excess relative permittivity of binary dielectrics. *Physical Chemistry Chemical Physics*, Vol. 11, 3977-3986.

Rivera-Rubero, S. & Baldelli, S. (2004). Surface spectroscopy of room-temperature ionic liquids on a platinum electrode: A sum frequency generation study. *Journal of Physical Chemistry B*, Vol. 108, 15133-15140.

Santos, V.O., Jr.; Alves, M.B.; Carvalho, M.S.; Suarez, P.A.Z. & Rubim, J.C. (2006). Surface-enhanced Raman scattering at the silver electrode/ionic liquid (BMIPF6) interface. *Journal of Physical Chemistry B*, Vol. 110, 20379-20385.

Scheutjens, J.M.H.M. & Fleer, G.J. (1979). Statistical theory of the adsorption of interacting chain molecules. 1. Partition function, segment density distribution, and adsorption isotherms. *Journal of Physical Chemistry*, Vol. 83, 1619-1635.

Scheutjens, J.M.H.M. & Fleer, G.J. (1980). Statistical theory of the adsorption of interacting chain molecules. 2. Train, loop, and tail size distribution. *Journal of Physical Chemistry*, Vol. 84, 178-190.

Simon, P. & Gogotsi, Y. (2008). Materials for electrochemical capacitors. *Nature Materials*, Vol. 7, 845-854.

Stillinger, F.H. & Kirkwood, J.G. (1960). Theory of the diffuse double layer. *Journal of Chemical Physics*, Vol. 33, 1282-1290.

Teschke, O. & de Souza, E.F. (1999). Dielectric exchange: The key repulsive or attractive transient forces between atomic force microscope tips and charged surfaces. *Applied Physics Letters*, Vol. 74, 1755-1757.

Thompson, R.B.; Ginzburg, V.V.; Matsen, M.W. & Balazs, A.C. (2001). Predicting the mesophases of copolymer-nanoparticle composites. *Science*, Vol. 292, 2469-2472.

Trulsson, M.; Algotsson, J.; Forsman, J.; Woodward, C.E. (2010). Differential capacitance of room temperature ionic liquids: the role of dispersion forces. *Journal of Physical Chemistry Letters*, Vol. 1, 1191-1195.

Valette, G. (1981). Double layer on silver single-crystal electrodes in contact with electrolytes having anions which present a slight specific adsorption. *Journal of Electroanalytical Chemistry*, Vol. 122, 285-297.

Yuan, Y.X.; Niu, T.C.; Xu, M.M.; Yao, J.L. & Gu, R.A. (2010). Probing the adsorption of methylimidazole at ionic liquids/Cu electrode interface by surface-enhanced Raman scattering spectroscopy. *Journal of Raman Spectroscopy*, Vol. 41, 516-523.

Ionic Liquids: Theory, Properties, New Approaches
Edited by Prof. Alexander Kokorin

ISBN 978-953-307-349-1
Hard cover, 738 pages
Publisher InTech
Published online 28, February, 2011
Published in print edition February, 2011

Ionic Liquids (ILs) are one of the most interesting and rapidly developing areas of modern physical chemistry, technologies and engineering. This book, consisting of 29 chapters gathered in 4 sections, reviews in detail and compiles information about some important physical-chemical properties of ILs and new practical approaches. This is the first book of a series of forthcoming publications on this field by this publisher. The first volume covers some aspects of synthesis, isolation, production, modification, the analysis methods and modeling to reveal the structures and properties of some room temperature ILs, as well as their new possible applications. The book will be of help to chemists, physicists, biologists, technologists and other experts in a variety of disciplines, both academic and industrial, as well as to students and PhD students. It may help to promote the progress in ILs development also.

InTech Europe
University Campus STeP Ri
Slavka Krautzeka 83/A
51000 Rijeka, Croatia
Phone: +385 (51) 770 447
Fax: +385 (51) 686 166
www.intechopen.com

InTech China
Unit 405, Office Block, Hotel Equatorial Shanghai
No.65, Yan An Road (West), Shanghai, 200040, China
中国上海市延安西路65号上海国际贵都大饭店办公楼405单元
Phone: +86-21-62489820
Fax: +86-21-62489821

IntechOpen